Proceedings World Geothermal Congress 2000
Kyushu - Tohoku, Japan, May 28 - June 10, 2000

X-RAY CT IMAGING OF PORES AND FRACTURES IN THE KAKKONDA GRANITE, NE JAPAN

Tomoyuki Ohtani, Yoshito Nakashima, Tsukasa Nakano and Hirofumi Muraoka
Geological Survey of Japan, Higashi, Tsukuba, 305-8567 Japan

Key Words*:* pores, fractures, X-ray computerized tomography, granite, Kakkonda geothermal field

ABSTRACT

Three-dimensional imaging of the Kakkonda granite from the borehole WD-1a was performed to clarify meso- and microscopic structures of pores and fractures in the geothermal reservoir by medical and industrial X-ray computerized tomography (CT) scanners. The granite was recovered from WD-1a drilled at the Kakkonda geothermal field, NE Japan, by the New Energy and Industrial Technological Development Organization (NEDO).

A third-generation Hitachi Medical Corporation CT-W2000 medical CT scanner enabled us to visualize millimeter-scale rock textures of the granite inside cores without any destruction. Miarolitic cavities, enclaves, felsic minerals (quartz and feldspar) and mafic minerals (biotite and hornblende) were identified from CT images. Three-dimensional distribution of miarolitic cavities was reconstructed from contiguous CT images and showed spatially heterogeneous distribution with the boundary that strikes N 20° E. Proportion of miarolitic cavities larger than 2 mm^3 was 0.33 /cm^3 between 2936.722 and 2936.921 m. Porosity calculated from X-ray CT images was 0.9 % from 2936.722 to 2936.821 m. We fitted ellipsoids with three arbitrary axes to the miarolitic cavities extracted from the contiguous CT images and examined aspect ratio and shape preferred orientations of ellipsoids. Fitted ellipsoids exhibit ellipsoidal shape and shortest axis trends to E-W. These indicate that these cavities may be deformed by the same regional stress as present one, which is E-W compression. The shape analysis of cavities would clarify the past deformational event.

A third-generation Nittetsu Elex Corporation ELE SCAN industrial CT scanner enabled us to visualize micron-scale microcracks in the granite. Microcracks are developed along grain boundary. These would be important to evaluate percolation and storage of the hydrothermal fluid in the granite.

1. INTRODUCTION

Understanding the distribution of the permeable zones in the geothermal field is important for the exploration and assessment of the reservoir. The distribution of the permeable zones such as pores and fractures is observed in the rock samples. These structures of the permeable zones would influence storage and percolation of the hydrothermal fluids.

The geothermal boreholes have penetrated young plutonic bodies in and beneath geothermal reservoirs at many geothermal fields in the world during the last two decades (Muraoka, 1993). For example, several boreholes confirmed the presence of a plutonic body in the deeper part of the Kakkonda geothermal field, NE Japan (Kato and Doi, 1993). The top of the plutonic body is expected to be a part of the geothermal reservoir (Muraoka, 1993).

The borehole WD-1a was drilled at the Kakkonda geothermal field (Fig. 1) as a part of the 'Deep-Seated Geothermal Resources Survey' project by the New Energy and Industrial Technological Development Organization (NEDO). Miarolitic cavities were found in the granite core recovered from WD-1a. These cavities may constitute a part of the geothermal reservoir in the granite, because several boreholes penetrating the granite encountered major lost circulation zones (Kato and Sato, 1995). Therefore, it is important to know the cavity characteristics such as three-dimensional distribution, size distribution, and shape characteristics.

X-ray computerized tomography (CT or CAT scanning) has been used in the medical field to image the human body for more than two decades (Hounsfield, 1973; Ledley et al., 1974). Recently, it has been applied to earth sciences. For instance, Bonner et al. (1994) confirmed fluid migration in the rock by X-ray CT. Chen et al. (1996) used X-ray CT in the experiment of air movement in sand with water. Tivey and Singh (1997) used X-ray CT to detail the internal structure of fragile sea-floor hydrothermal vent samples. Nakashima et al. (1997) applied X-ray CT to the three-dimensional non-destructive imaging of arrays of fluid inclusions in a mineral. Ohtani et al. (1997) and Ohtani et al. (in press) used X-ray CT to clarify the heterogeneous distribution of miarolitic cavities in granite. We describe here the result of three-dimensional imaging of millimeter-scale miarolitic cavities in a granite core from WD-1a and discuss the relationship between the structure of cavity and the geothermal reservoir. We also tried to visualize micron-order microcracks by X-ray CT, because permeable structures consist of not only millimeter-scale cavities but also micron-order microcracks.

2. SAMPLE DESCRIPTION

The borehole WD-1a is located at the Kakkonda geothermal field, NE Japan. The hole was 3729 m deep. WD-1a penetrated the Quaternary and Tertiary volcanic rocks and the pre-Tertiary sedimentary rocks, and encountered the Kakkonda granite, which is presumed to be a heat source of the Kakkonda geothermal field, at 2860 m depth (Kato et al., 1996) (Fig. 2). The temperature was more than 500 ºC at the bottom of the hole (Ikeuchi et al., 1996; Kato et al., 1996). The K-Ar age of biotite ranges from 0.068 to 0.34 Ma (Kanisawa et al., 1994). WD-1a provided four spot cores from the Kakkonda granite. The diameter of the core is 10.15 cm. Miarolitic cavities were found from 2936.4 to 2937.6 m in the spot core from 2936.0 to 2939.0 m depth.

The target for the CT imaging in this study is the miarolitic cavities and microcracks in the Kakkonda granite. The sample is a medium- to fine-grained weakly porphylitic granodiorite with miarolitic cavities of a few mm in diameter. Quartz and plagioclase grains as phenocrysts exhibit euhedral. Their grain size is the range from 0.7 to 4.5 mm. Quartz, plagioclase, and potassium feldspar in ground mass exhibit anhedral to subhedral, and their grain size ranges from 0.1 to 0.7 mm. Enclaves with diameter 5 to 40 mm exist sporadically as aggregates of mafic minerals.

3. PROCEDURE OF X-RAY COMPUTERIZED TOMOGRAPHY

X-ray CT reconstructs internal images from the distribution of the X-ray absorption coefficient inside the sample deduced from the projection of X-ray through a sample. The X-ray absorption coefficient is usually called CT number (χ) defined as

$$\chi = (\nu-\nu_0) / \nu_0 \times 1000$$

where ν is the linear attenuation of the sample and ν_0 is the linear attenuation of the standard reference. In hospital applications water is normally used as a standard reference for scanning human tissue. In mesoscopic observation, the same definition of CT number as hospital application was used. The CT number of water appears with a value of 0, and that of nonattenuating material like air appears with a value of -1000. The CT number is a function of the average density and composition of the material in any voxel. For example, the CT number increases gradually in order of air, water, felsic minerals, biotite, hornblende and pyrite. This indicates that X-ray CT enables us to do non-destructive imaging of minerals with different density in the rock.

A third-generation Hitachi Medical Corporation CT-W2000 CT scanner was used for mesoscopic observation. This scanner is equipped with an X-ray emission source and 768 elements of X-ray detector (Fig. 3). The performance of this scanner is 0.75 mm for spatial resolution, 1mm for minimum slice thickness, 130 kV for maximum voltage of the X-ray tube, and 160 mm for minimum imaging diameter.

The procedure of the CT imaging was as follows. First, we took contiguous CT images at intervals of 1 mm. The imaging condition is 1.0 mm for slice thickness, 0.313 × 0.313 × 1 mm for voxel size, 4.0 seconds for scan time, 175 mA for X-ray tube current, 130 kV for X-ray tube voltage, 160 mm for imaging diameter, and 512 × 512 for matrix size. The CT imaging of 99 slices took 53 minutes. Second, three-dimensional image of the sample was reconstructed by Macintosh software 'Fortner Slicer'. This software enabled us to visualize three-dimensional cavity distribution. Third, volume measurement and ellipsoid fitting were performed. Axes orientations and aspect ratios of ellipsoids fitted to the miarolitic cavities were estimated.

A third-generation Nittetsu Elex ELE-SCAN NX-NCP-C80-I4 industrial CT scanner was used for microscopic observation. This scanner equipped with an X-ray emission source and 1024 linear sensors of X-ray detector, and in-plane resolution is 5.05 μm. The imaging condition is 8.08 μm for slice thickness, 5.05 × 5.05 × 8.08 μm for voxel size, 100 μA for X-ray tube current, 46 kV for X-ray tube voltage, 5.2 mm for imaging diameter, and 1024 × 1024 for matrix size. The CT imaging of 200 slices took 60 minutes.

4. TWO-DIMENSIONAL OBSERVATION OF X-RAY CT IMAGES

4.1 Mesoscopic observation

Some CT images were compared with cutting surface of the core to identify the CT image as rock textures. Voxels with CT number less than 1540 correspond to the miarolitic cavities in the granite (a in Fig. 4). The enclaves are recognized as aggregates of voxels with CT number more than 2350 (b in Fig. 4). Voxels with CT number more than 2350 correspond to the coarse mafic minerals (c in Fig. 4). The fine mafic minerals have lower CT number than the coarse ones. This results from the influence of the surrounding minerals with low CT number. Voxels with CT number from 1540 to 2350 except fine mafic minerals correspond to quartz and feldspar. The three traces of the scribe knife carved on the core surface are recognized, since this core is oriented.

4.2 Microscopic observation

We tried to visualize microcracks using two ways of CT imaging. First, we took CT images of a cylindrical sample (ϕ5mm×10mm) from a granite core. Grains exhibit several CT numbers (Fig. 5a). This may indicate different minerals. Textures such as microcracks are not recognized. The reason would be that the thickness of microcracks is less than in-plane resolution of X-ray CT. Next, saturated KI solution was infiltrated into the sample. Nakashima (in press) showed that KI solution greatly increases the CT number. To infiltrate KI solution, the sample was vacuumed in saturated KI solution for several hours, and then it was put in the same KI solution under atmospheric pressure. The KI solution filled microcracks were detected by X-ray CT (Fig. 5b). Microcracks exhibit as voxels with a CT number higher than those of surrounding minerals, because KI solution infiltrated into microcracks shows a high CT number. Microcracks are developed along grain boundaries.

5. THREE-DIMENSIONAL ANALYSIS OF X-RAY CT IMAGES

5.1 Cavity distribution

The stacking of the two-dimensional CT slice images enables us to view the three-dimensional objects. Fig. 6 shows the three-dimensional distribution of miarolitic cavities in the core. The air surrounding the granite core and voxels with a CT number more than 1540 are made transparent, hence the distribution of voxels with the CT number less than 1540 in the granite core is visualized. The voxels with the CT number less than 1540 inside the granite correspond to the miarolitic cavities.

Fig. 7 shows perspectives of granite and visualizes miarolitic cavities from top, south and west. Only small cavities are recognized from 2936.040 to 2936.136 m. Large cavities develop with the inclined boundary from 2936.350 to 2936.446 m. The apparent boundary of two kinds of cavities strikes N 16° E as shown solid lines in Fig. 7b. As corrected by drilling azimuth S 72.23° W and dip 10.27° at 2940 m depth of WD-1a (NEDO, 1996a), the true boundary is N 20° E. Large cavities develop widely in 2936.822 to 2937.120 m. The boundary of large cavities appears again in 2937.121 to 2937.220m. Thus, we conducted that the large cavities existed between 2936.350 and 2937.220 m on the basis of the cavity distribution

5.2 Cavity size distribution

Cavity size distribution was calculated by the computer program of Watanabe et al. (1999). This program checks the connectivity of adjacent voxels, carries out cluster labeling and calculates the volume of each cluster. The results of the calculation are shown in Fig. 8. Although the cavities smaller than 2mm^3 are abundant in each interval, these may contain noise and error of the X-ray CT. A few small cavities appear in the interval from 2936.04 to 2936.14 m. Above 2936.722 m, the cavities larger than 50 mm^3 are very few and the total

number of cavities increases downward. The total number of cavities is the greatest between 2936.722 and 2936.921 m and the proportion of cavities larger than 2 mm^3 is 0.33 /cm^3 in this interval. Below 2936.921 m, the total number of cavities decreases downward slightly.

5.3 Porosity

Porosity of the Kakkonda granite was estimated from X-ray CT images as the ratio of the voxels with the CT number less than 1540 to those of the entire core. The estimated porosity was 0.02, 0.1 % in 2936.040 - 2936.136 m and 2936.350 - 2936.446 m and 0.9, 0.7, 0.4, 0.5 and 0.5 % in each 0.1 m from 2936.722 to 2937.220 m respectively.

5.4 Cavity shape analysis

The shape of miarolitic cavities was estimated from the contiguous CT images stacked at intervals of 1 mm by computer programs (Ikeda et al., in press). These programs analyze connectivity of voxels with CT number between given lower and upper values and perform cluster labeling of reconstructed objects. Next, a program fits ellipsoids with three arbitrary axes to these objects (Fig. 9) and outputs lengths and directions of axes of each ellipsoid. The objects with length parallel to the longitudinal axis of core shorter than 3 voxels were excluded from the analysis, because such objects are too small to fit ellisoids.

The shortest (a), intermediate (b) and longest (c) axes of ellipsoids fitted to miarolitic cavities prefer to E-W, N-S and vertical respectively (Fig. 10). The flinn diagram (Flinn, 1962) indicates most cavities exhibit the shape of plane strain type (Fig. 11). Although a few cavities seem to show prolate type, these may connect some cavities.

6. DISCUSSION

We performed X-ray CT imaging of the Kakkonda granite and estimated the spatial distribution and morphological characteristics of the miarolitic cavities. The boundary of small and large cavities was confirmed from Fig. 7, although it was difficult to estimate cavity distribution from core surface observation. Three-dimensional X-ray CT imaging enabled us to visualize the structure of aggregate such as miarolitic cavity zone.

The large cavity zone develops in the direction of N 20° E. This trend is consistent with that of the low-resistive zone (NEDO, 1996a) and isothermal contour at 500 m below sea level (Tamanyu, 1994) and the hypocenter distribution of microearthquakes in shallow depth from the Kakkonda granite (Uchida et al., 1996). As the high-porosity zone such as the miarolitic cavity zone may develop into the geothermal reservoir, the direction of N 20° E may be a trend governing the geothermal reservoir in the Kakkonda geothermal field.

Cavity size distribution (Fig. 8) indicates that large cavities are developed in depths where many cavities are scattered. The large and high-density cavity zone is limited below 2936.772 m depth. Although the maximum cavity size is estimated to be 250 mm^3, we must recognize the possibility that the apparent cavity size estimated by the X-ray CT is larger than the true size because the cavities may appear to be connected to the neighboring cavities because of the resolution size of the X-ray CT.

The porosity of the Kakkonda granite estimated from the CT image is lower than that from conventional method. NEDO (1996b) reported the porosity of the Kakkonda granite with no mesoscopic cavities is 1.98 % by water saturation method. The porosity reported by NEDO (1996b) is quite different from 0.02 % by X-ray CT. This difference results from the resolution of X-ray CT. Although the cavities with a few mm of diameter are detectable by medical X-ray CT used in this study, microcracks cannot be detected because of the spatial resolution of the medical X-ray CT. Thus the porosity estimated from X-ray CT would indicates a ratio of miarolitic cavities in the samples.

The industrial X-ray CT visualized grain boundary cracks. Fujimoto et al. (1998) showed from scanning electron microscope observation and permeability tests that grain boundary of the Kakkonda granite is not close and the permeability is higher than other granites. These grain boundary cracks may be part of the storage of hydrothermal fluids. As the granite samples, however, were recovered from the deeper part with high temperature, we must consider the effect of stress release and thermal expansion for propagating grain boundary cracks.

Preferred axial orientations of ellipsoids fitted to miarolitic cavities may be explained by the regional compression. The present regional stress field in NE Japan is E-W compression and reverse fault type (Shimazaki et al., 1978). One possible reason why the shortest (a) axis of ellipsoids fitted to the miarolitic cavities trends E-W is that the cavities were deformed by the same regional stress as the present one and cavities were shortened from the E-W direction. Although the timing of cavity deformation is uncertain, the paleostress field would be similar to the present one. Because the Kakkonda granite is so young the regional stress field is assumed not to change since the emplacement of the granite. Sato (1994) reported that the regional stress field in NE Japan has been constant since 3.5 Ma.

Molten magma can not hold differential stress. The present stress state in the Kakkonda granite is shown from differential strain curve analysis (DSCA) (NEDO, 1996a) and drilling induced fractures (Doi et al., 1997). DSCA indicates that the amount of differential stress decrease toward the deeper part. The estimated differential stress from DSCA that σ_3 / σ_1 at the 1000 m depth in volcanic rock and 2937 m depth in plutonic rock are 0.17 and 0.64 respectively. However, the development of drilling induced fractures was observed over the whole depth from volcanic rocks to plutonic rocks along the WD-1b which is a side-tracked borehole and this indicated that E-W compression is dominant. As the formation of drilling induced fractures needs large differential stress and drilling induced fractures as an in-situ measurement is more reliable than DSCA as a laboratory experiment, the present stress state in the Kakkonda granite would be E-W compressional with large differential stress. As some granite plutons exhibit magmatic foliation (cf. Ramsay, 1989), granitic magma would hold differential stress.

ACKNOWLEDGEMENTS
We thank the New Energy and Industrial Technology Development Organization (NEDO) for their permission to use core samples and publish this paper. Orientation data

were plotted using Stereonet v.4.9.6 by Richard W. Allmendinger, Cornell University. This research was supported by the New Sunshine Project (Deep-Seated Geothermal Resources Survey) of Ministry of International Trade and Industry, Japan.

REFERENCES

Bonner, B. P., Roberts, J. J., and Schneberk, D. J. (1994). Determining water content and distribution in reservoir graywacke from the northeast Geysers with X-ray computed tomography. *Geotherm. Resour. Coun. Trans.*, Vol.18, pp.305-310.

Chen, M. R., Hinkley, R. E., and Killough, J. E. (1996). Computed tomography imaging of air sparging in porous media. *Water Resour. Res*., Vol.32, pp.3013-3024.

Doi, N., Kato, O., Sakagawa, Y., Akaku, K. and Uchida, T. (1997). Characterization of fracture and rock property of the Kakkonda granite by FMI and other loggings. *Jnl. Geotherm. Res. Soc. Japan*, Vol.20, pp.34 (in Japanese).

Flinn, D. (1962). On folding during three-dimensional progressive deformation. *Geol. Soc. Lond. Quar. Jnl.* Vol.118, pp.385-433.

Fujimoto, K., Takahashi, M., Doi, N., and Kato, O. (1998). High permeabilities of Quaternary granites in Japan and its implications for mass and heat transfer in a magmatic-hydrothermal system. *Proc. 9th Int. Symp. on water-rock interaction,* pp.227-230.

Hounsfield, G. N. (1973) Computerized transverse axial scanning (tomography), 1, Description of system. *British Jnl. Radiology*, Vol.46, pp.1016-1022.

Ikeda, S., Nakano, T., and Nakashima, Y., (in press). Three-dimensional study on the interconnection and shape of crystals in a graphic granite by X-ray CT and image analysis. *Miner. Mag.*

Ikeuchi, K., Komatsu, R., Doi, N., Sakagawa, Y., Sasaki, M., Kamenosono, H., and Uchida, T. (1996). Bottom of hydrothermal convection found by temperature measurements above 500ºC and fluid Inclusion study of WD-1 in Kakkonda geothermal field, Japan. *Geotherm. Resour. Coun. Trans*., Vol.20, pp.609-616.

Kanisawa, S., Doi, N., Kato, O., and Ishikawa, K. (1994). Quaternary Kakkonda granite underlying the Kakkonda geothermal field, Northeast Japan. *Jnl. Min. Petr. Econ. Geol*., Vol.89, pp.390-407 (in Japanese with English abstract).

Kasai, K., Sakagawa, Y., Komatsu, R., Sasaki, M., Akaku, K., and Uchida, T. (1998). The origin of hypersaline liquid in the Quaternary Kakkonda granite, sampled from well WD-1a, Kakkonda geothermal system, Japan. *Geothermics*, Vol.27 (5/6), pp.631-645.

Kato, O., and Doi. N. (1993). Neo-granitic pluton and late hydrothermal alteration at the Kakkonda geothermal field, Japan. *Proc. 15th NZ Geothermal Workshop 1993*, pp.155-161.

Kato, O., and Sato, K. (1995). Development of deep-seated geothermal reservoir bringing the Quaternary granite into focus in the Kakkonda geothermal field, Northeast Japan. *Resource Geol*., Vol.45 (3), pp.131-144. (in Japanese with English abstract).

Kato, O., Doi, N., Ikeuchi, K., Kondo, T., Kamenosono, H., Yagi, M., and Uchida, T. (1996). Characteristics of temperature curves and fracture systems in Quaternary granite and Tertiary pyroclastic rocks of NEDO WD-1a in the Kakkonda geothermal field, Japan. *Proc. 8th Int. Symp. on the Observation of the Continental Crust Through Drilling*, pp.241-246.

Ledley, R. S., Chiro, G. D., Luessenhop, A. J., and Twigg, H. L. (1974). Computerized transaxial X-ray tomography of the human body. *Science*, Vol.186, pp.207-212.

Muraoka, H. (1993). Scope of the future geothermal resources from the viewpoint of magma. *Chinetsu (Jnl. Japan Geotherm. Ener. Assoc.)*, Vol.30, pp.100-126 (in Japanese).

Nakashima, Y., Hirai, H., Koishikawa, A., and Ohtani, T. (1997). Three-dimensional imaging of arrays of fluid inclusions in fluorite by high-resolution X-ray CT. *N. Jb. fur Miner. Mh*., 1997(12), pp.559-568.

Nakashima, Y. (in press). The use of X-ray CT to measure diffusion coefficients of heavy ions in water-saturated porous media. *Eng. Geol*.

NEDO (1996a). FY 1995 report of the Deep Geothermal Resources Survey Project. 887pp. (in Japanese with English abstract).

NEDO (1996b). FY 1994 report of the Deep Geothermal Resources Survey Project. 567pp. (in Japanese with English abstract).

Ohtani, T., Nakashima, Y., and Muraoka, H. (1997). Three-dimensional imaging of textures in the Kakkonda granite using X-ray CT. *Jnl. Geotherm. Res. Soc. Japan*, Vol.19 (4), pp.209-216 (in Japanese with English abstract).

Ohtani, T., Nakashima, Y., and Muraoka, H. (in press). Three-dimensional miarolitic cavity distribution in the Kakkonda granite from borehole WD-1a using X-ray computerized tomography. *Eng. Geol.*

Ramsay, J.G. (1989). Emplacement kinematics of a granite diapir: the Chindamora batholith, Zimbabwe. *Jnl. Struct. Geol*. Vol.11 (1/2), pp.191-209.

Sato, H. (1994). The relationship between late Cenozoic tectonic events and stress field and basin development in northeast Japan. *Jnl. Geophys. Res*., Vol.99 (B11), pp.22261-22274.

Shimazaki, K., Kato, T., and Yamashita, K. (1978). Basic types of internal deformation of the continental plate at arc-arc junctions. *Jnl. Phys. Earth*, Vol.26, Suppl., pp.S66-S83.

Tamanyu, S. (1994). Magma reservoirs from the viewpoint of geothermal modeling: Examples from the Hohi, Sengan and Kurikoma geothermal areas in Japan. *Mem. Geol. Soc. Japan*, Vol.43, pp.141-155 (in Japanese with English abstract).

Tivey, M. K., and Singh, S. (1997) Nondestructive imaging of fragile sea-floor vent deposit samples. *Geology*, Vol.25, pp.931-934.

Uchida, T., Akaku, K., Sasaki, M., Kamenosono, H., Doi, N., and Miyazaki, S. (1996). Recent progress of NEDO's "Deep-seated Geothermal Resources Survey" project. *Trans Geotherm. Res. Coun*., Vol.20, pp.643-648.

Watanabe, Y., Nakashima, Y., and Ohtani, T. (1999). 3D-image processing program for the calculation of the volume histogram of cavities in rock samples. *Jnl. Geotherm. Res. Soc. Japan*, Vol.21 (2), pp.181-188.

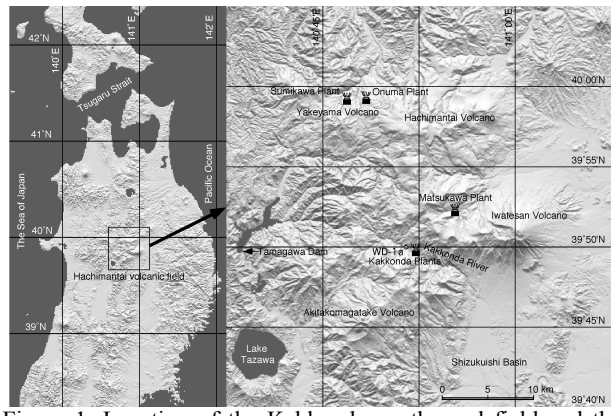

Figure 1. Location of the Kakkonda geothermal field and the drill site of the borehole WD-1a.

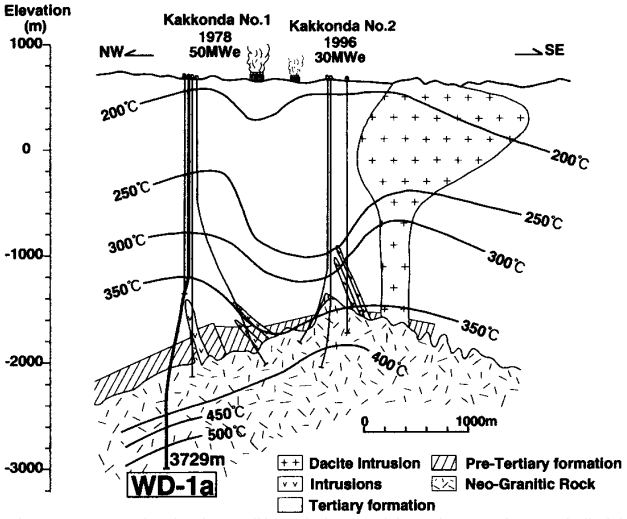

Figure 2. Geological profile of the Kakkonda geothermal field and the traces of WD-1a and WD-1b (modified from Kato et al., 1996 and Kasai et al., 1998).

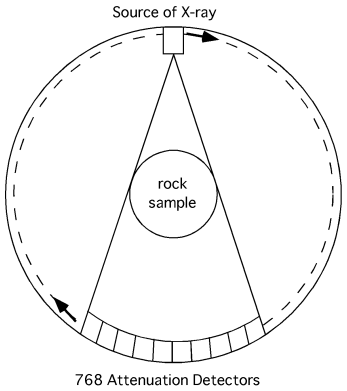

Figure 3. Outline of third-generation X-ray CT scanner

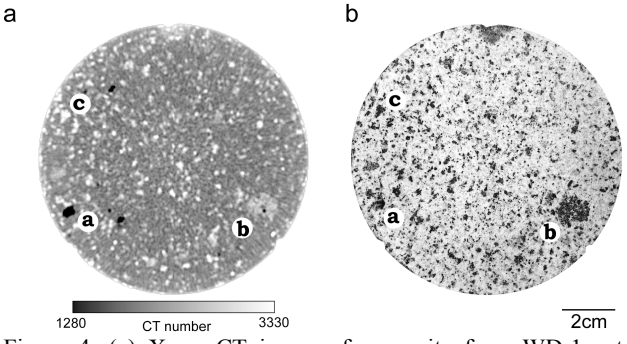

Figure 4. (a) X-ray CT image of a granite from WD-1a at 2936.445 m depth. (b) The photograph of polished surface. The slice positions of a and b are identical to each other. Both images are taken from downside. a: Miarolitic cavity, b: Enclave, c: Mafic mineral.

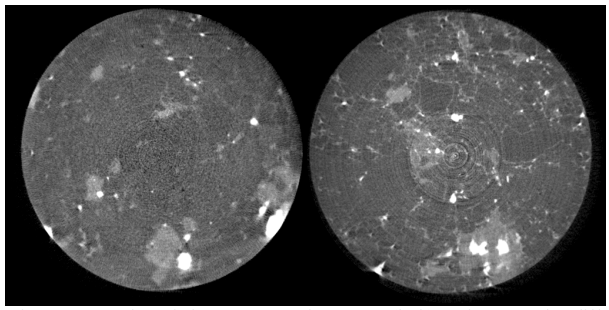

Figure 5. Industrial X-ray CT images. (left) Microcracks filled by air. (right) Microcracks enhanced by saturated KI solution.

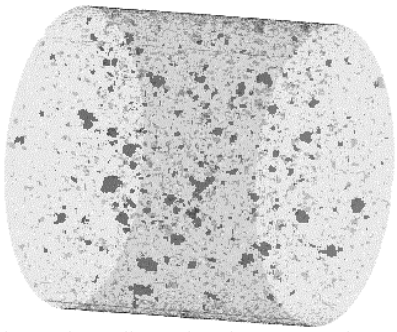

Figure 6. Binary three-dimensional X-ray CT image. Gray and light gray indicate the miarolitic cavities and the surface of core sample, respectively. The diameter and length of the core sample is 10.15 cm and 9.6 cm, respectively.

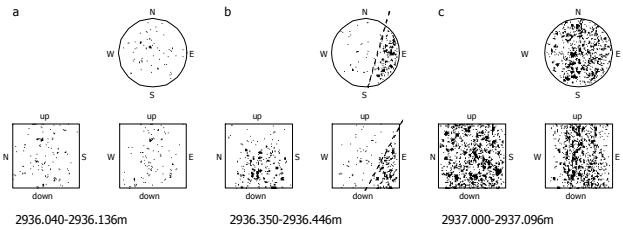

Figure 7. Binary perspectives of miarolitic cavities from upside (left), south (center) and west (right). Solid lines indicate the boundary of small and large cavities.

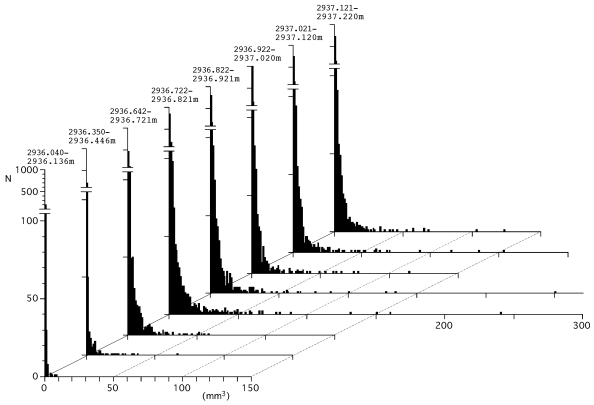

Figure 8. Histogram of cavity size distribution.

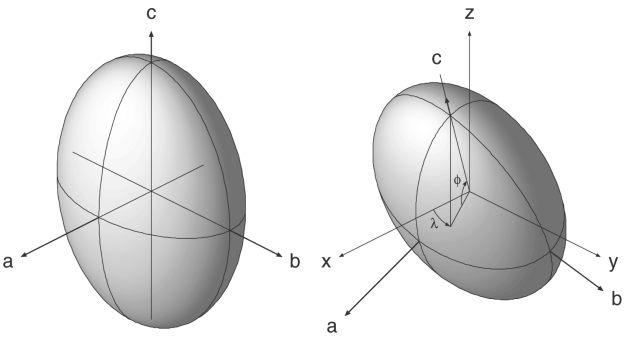

Figure 9. Schematic images of fitted ellipsoids and their axes.

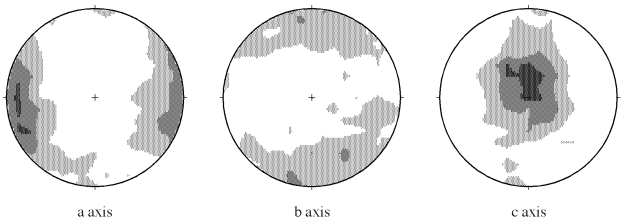

Figure 10. Axial distribution of ellipsoids fitted to miarolitic cavities. N = 1285. Equal area and lower hemisphere projection. Contour interval is 1.0 %/1% area.

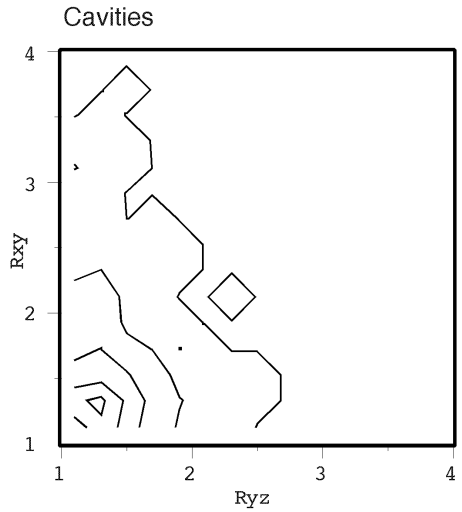

Figure 11. Flinn diagrams showing the shape of miarolitic cavities. Contour is 0.1, 10, 50, 100, 150 /0.2*0.2 area.